Excitation-Emission Matrix Spectroscopy for Analysis of Chemical Composition of Combustion Generated Particulate Matter

*Gaurav Mahamuni[1], Jay Rutherford[2], Justin Davis[3], Eric Molnar[1], Jonathan D. Posner [1,2], Edmund Seto[5], Gregory Korshin[4], Igor Novosselov[1,5,6]

[1] University of Washington, Mechanical Engineering, Seattle, WA 98195

[2] University of Washington, Chemical Engineering, Seattle, WA 98195

[3] University of Washington, Molecular Engineering, Seattle, WA 98195

[4] University of Washington, Civil and Environmental Engineering, Seattle, WA 98195

[5]University of Washington, Environmental and Occupational Health Sciences, Seattle, WA 98195

[6]University of Washington, Institute for Nano-Engineered Systems, Seattle, WA 98195

*Corresponding Author Email: gauravsm@uw.edu

1. Graphical Abstract

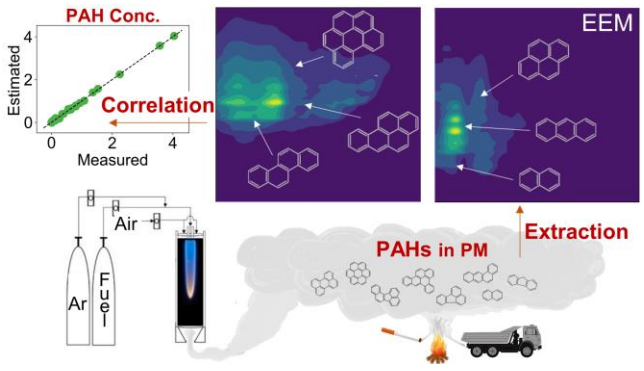

2. Abstract

Analysis of particulate matter (PM) is critical for the assessment of human exposures to potentially harmful agents, notably combustion-generated PM; specifically polycyclic aromatic hydrocarbons

(PAHs) found in them and associated with carcinogenic and mutagenic effects. In this study, we quantify the presence and concentrations of PAHs with low molecular weight (LMW, 126<MW<202) and higher molecular weight (HMW, 226<MW<302) in combustion-generated PM using excitation-emission matrix (EEM) fluorescence spectroscopy. PM samples were generated in a laminar diffusion inverted gravity flame reactor (IGFR) operated on ethylene and ethane. Fuel dilution by Ar in 0% to 90% range controls the flame temperature. The colder flames result in lower PM yields; however, the PM PAH content increases significantly. Temperature thresholds for PM transition from low to high organic carbon content were characterized on the basis of the maximum flame temperature ($T_{max,c}$ ~1814-1864K) and highest soot luminosity region temperature (T^*_c~1600-1650K). Principal component regression (PCR) analysis of the EEM spectra correlates to GCMS data with R^2 values of 0.98 for LMW and 0.99 for HMW PAHs. The agreement demonstrates that PCR-EEM analysis can be used to determine relative concentrations of organic carbon and PAH fraction in combustion PM.

3. Introduction

Ultrafine PM can originate from mobile and industrial combustion sources, forest fires, and other natural and anthropogenic sources. Size distributions, particle morphology, optical properties, and chemical composition of these aerosols vary significantly.[1–5] Environmental and occupational exposures to combustion PM have been linked to adverse effects on human health. Air pollution was shown to be responsible for 4.2 million deaths in the year 2016.[6] The toxic potential of PM exposure depends on particle size and chemical composition.[7,8] It is important to evaluate the organic composition in PM from combustion sources to study the health effects of PM exposure[9]; however, in large epidemiological studies, it is challenging and costly to perform detailed chemical analyses of the collected samples.[10,11] Therefore, there is a need for robust, low-cost methods for

analysis of PM chemical composition for improved health risk assessment, guidance for the management of diseases, and targeted intervention strategies.

Of particular interest is the role of combustion generated PAHs as their exposure has been associated with carcinogenic and mutagenic activity in humans.[12–14] In the environment PAHs can exist in a vapor phase or be associated with airborne PM depending on the atmospheric conditions, the nature of the aerosol (i.e., origin and properties), and the properties of the PAH.[15,16] Combustion generated PM consists of graphitic structures and an organic fraction that varies with flame conditions and fuel composition. PM formed by the combustion process follows certain growth, maturation, and aggregation pathways. First, fuel pyrolysis and entropic-driven chemical reactions form PAHs, which are stable in the fuel-rich flame environment. [13,14] These PAHs grow in size building clusters[19], which leads to the creation of nascent soot particles.[20,21] The nascent soot grows by hydrogen abstraction-carbon addition (HACA) or by condensation mechanisms.[20] Secondary growth of soot particles is possible in complex flow field scenarios.[22] The PAHs participating in PM formation can be oxidized before the particle exits the flame; however, depending on the combustion conditions, a significant fraction of organic compounds can be retained by the particle.

Total organic carbon (TOC) analysis is a widely used, relatively low-cost method for estimation of the organic fraction in PM samples.[23,24] Variations in the organic fraction of the ultrafine PM leads to uncertainty of the PM exposure impact on health.[10,25] Though the organic fraction in combustion PM contains a variety of complex hydrocarbon compounds[5], among them, PAHs have been reported to be a major cause of oxidative damage.[26–28] The Environmental Protection Agency (EPA) has established a panel of 16 PAH compounds as priority pollutants that represent a range of molecular structures with 128<MW<278 g/mol.[29] More recent reports[30] show that among these,

higher molecular weight (HMW) PAHs have high cancerogenic potential. The majority of these HMW PAHs are classified as probably or possibly carcinogenic (groups 2A and 2B, respectively), and Benzo-a-pyrene is classified as carcinogenic (group 1) by the International Agency for Research on Cancer (IARC).[31] The lower molecular weight (LMW) PAHs are considered non-genotoxic, except naphthalene;[31,32] however, these LMW PAHs can be acutely toxic.[33]

PAH analysis in PM is performed via gas chromatography-mass spectrometry (GCMS) and liquid chromatography-mass spectrometry (LCMS)[34–38], both techniques are labor-intensive and require expensive equipment. New spectroscopy-based technologies are being developed to complement the conventional analysis techniques to determine the PM PAH content.[39–46] PAHs are good candidates for detection by spectroscopic techniques as they have high absorption coefficients and quantum yields.[47] The UV–visible electronic transitions in sp^2 carbon systems such as PAHs rely on $\pi*$–π transitions.[48] Several studies show that there is an inverse power law relationship between the optical band gap (OBG) and the number of benzene rings in PAHs[49,50]. An increase in MW of PAHs broadens their absorption bands towards longer wavelengths and red-shifts their emission bands due to the decreasing OBG.[51,52] This variation in spectral properties as a function of MW can be used to distinguish PAH content in combustion aerosols. In general, fluorescence spectroscopy is highly sensitive (~1ng/mL) for PAH detection in ultrafine PM[53–55]; however, it is not specific. For analysis of multi-component mixtures, scanning single-wavelength-excitations and stacking fluorescence emissions at each excitation wavelength provides a three-dimensional spectral fingerprint of the sample known as Excitation Emission Matrix (EEM). EEM analysis has been used previously for PM source identification[56], PAH content in liquid samples, and qualitative analysis of diesel spray.[57–61] However, a convolution of individual compound signatures in a multi-component mixture, such as environmental samples, generates complex EEM

spectra that are difficult to interpret. Multivariate statistical techniques can be used to decompose the EEMs.[62,63]

In this study, we demonstrate the ability of EEM technique coupled with multivariate statistical analysis to estimate concentrations of PAH fractions in combustion PM. The PM samples with varied TOC fractions were generated by the combustion of diluted ethylene and ethane fuels in an inverted gravity flame reactor (IGFR)[64]. These samples were analyzed for soot yields, TOC, and PAH fraction. Concentrations of 24 PAHs with 128<MW<302 g/mol were measured using GCMS. Based on their MW, the PAHs were categorized as LMW PAHs (MW=128-202 g/mol) or HMW PAHs (MW=226-302 g/mol). EEM analysis coupled with principal component regression (PCR) was performed in parallel to develop a model for estimation of LMW and HMW PAH fractions in PM. The PCR-EEM estimates show excellent correlations (R^2~0.98-0.99) with PAH concentrations measured by GCMS for the two ranges of MWs. This technique can be used as a sensitive, low-cost alternative to TOC or GCMS analyses of PM.

4. Experimental Methods

4.1. PM Collection in Inverted Gravity Flame Reactor (IGFR)

An IGFR can generate ultrafine PM with a wide range of combustion temperatures due to the stable flame and high residence time compared to an upright flame. The IGFR allows for control of flame residence times (τ_{res}) by altering the balance of the convective and buoyant terms.[65] The increased residence time and flame stability in the IGFR have been utilized to synthesize materials such as carbon and TiO_2 aerosol gels[66,67] and for testing of several hypotheses related to PM formation and growth.[22] Here, the IGFR is used to produce combustion PM samples with controlled organic carbon fraction by varying the flame temperature with fuel dilution by Ar. The

IGFR consists of a 150 mm long quartz tube with an inner diameter of 32 mm. A mixture of fuel and Ar enters the combustor in a "+g" (downward) direction. The air is introduced as a co-flow into the reactor via concentric inlets having diameters 9.5 mm and 32 mm. A flow straightener at the combustor inlet prevents the propagation of instabilities from the air manifold.

The combustion conditions, such as temperature, dilution, fuel composition, and flowrates determine the PM formation rates and routes, thus controlling PAH fractions in the sample. The dilution ratio is defined as the ratio of Ar to the fuel-Ar mixture flow rate on volumetric basis. Introduction of Ar reduces the maximum flame temperature (T_{max}). For each fuel, the overall fuel-air equivalence ratio (φ) was kept constant. Figure S1 shows the IGFR schematic, and Figure S2 shows engineering drawings of the reactor. Table S1 shows the experimental conditions matrix. Note that T_{max} generally does not correspond to the region of the maximum soot production.[68] The soot formation region temperature (T^*) is a more relevant measure for particle exposure to temperature. Methodology for finding T^* is based on the flame luminosity in the red spectra.[68] Due to the uncertainties in estimating the range and location of T^* (as shown in SI Section 4), we use T_{max} for flame characterization, T^* is also reported for reference, the typical values are lower than T_{max} by 50-300K.

The soot emission factor, defined as mg of PM per gram of fuel, was calculated by gravimetric analysis. Zeflour PTFE filters (Pall Zefluor®, Pall Cat. # P5PJ037) were weighed before collection using a microbalance with 0.5 µg resolution (Mettler-Toledo UMT-2, Greifensee, Switzerland).[69] A weighed filter was placed in an open-face filter holder downstream of the flame. The sampling flow rate was set at 4 slpm, which was greater than the inlet flow, to assure all PM was collected. Make-up air compensated for the difference in inlet and sampling flow rates. The sample collection time was varied according to PM yields to gain an adequate mass for TOC, GCMS, and EEM

analyses. Table S1 shows the number of replicates for each condition. TOC analysis was performed by Sunset Laboratories Inc (Tigard, OR-97223, USA) using a thermal/optical method based on NIOSH 5040.[70]

4.2. Sample Extraction

After the gravimetric analysis, the samples were extracted in cyclohexane (Uvasol® Cyclohexane for Spectroscopy, MilliporeSigma Cat. #1.02822.2500). The filters were cut into four equal parts, and placed in 20 mL glass vials (Cat # 89096-774 VWR, Edison, NJ). The vials were filled with ~3mL of cyclohexane and sonicated for 30 min in a water bath sonicator (42 kHz, 2510R-MT Branson, Ultrasonic Corp., Danbury, CT). After sonication, the samples were soaked for 24 hours and filtered with 0.2 µm PTFE syringe filters (VWR Cat. #28145-491) into 4 mL vials (Cat # 66009-876 VWR, Edison, NJ). Blank filters, used for reference, were extracted in the same manner. Aliquots (200 µL) of filtered extracts were transferred into 2 mL GCMS vials having 250 µL inserts and PTFE screw tops (Cat# 5182-0715, 5181-8872 and 5182-0717, Agilent, Santa Clara, CA) for GCMS analysis. The remaining extracts were diluted further into 20 mL glass vials to a final concentration of 40 µg(soot)/mL(cyclohexane) for EEM analysis.

4.3. Gas Chromatography-Mass Spectroscopy (GCMS) Analysis

The extracts were analyzed using an Agilent 7000 GC/MS Triple Quad Mass Spectrometer using two 15 m columns (Agilent Part #: HP-5MS UI) equipped with a backflush. 24 PAHs (EPA 16 PAHs[29] and eight additional compounds with MW up to 302 g/mol) were included in the analysis, see Figure S5. Calibration curves for PAH species with seven concentration levels in the range 1-1000 ng/mL were obtained. The calibration standards for the 24 PAHs were a mixture of 23 compounds (Wellington Laboratories Cat. # PAH-STK-A, Guelph, ON, Canada) and one

additional compound, coronene, a standard PAH used in several studies on mechanisms of soot formation[20] (AccuStandard Cat. # H-116, New Haven, CT, USA). Each calibrant included 16 deuterium-labeled PAH internal standards (Wellington Laboratories Cat. # PAH-LCS-A, Guelph, ON, Canada). PAH internal standards were at a concentration of 100 ng/mL in the calibrants, and an equivalent concentration of the same internal standard was spiked into each sample for use in quantification. SI Section 5 shows the compounds and calibration curve details. The instrument was operated in pseudo multiple reaction monitoring (PMRM) mode,[71] the details are provided in SI Section 5.

4.4. Excitation-Emission Matrix (EEM) Analysis

The EEM spectra of PM extract samples, each having a concentration of 40 μg(soot)/mL(cyclohexane), were obtained using a spectrofluorometer (Aqualog-880-C, HORIBA Instruments Inc. Edison, NJ). The spectra were recorded in the range of excitation wavelength λ_{ex} = 200-600 nm with a 2 nm resolution. For each excitation wavelength, the instrument records emissions using CCD array in the range of λ_{em} = 246-826 nm with a 0.58 nm resolution. The spectra were normalized to Raman units (R.U.).[72] To account for Rayleigh scattering, an EEM of blank cyclohexane was subtracted from each EEM sample. The remaining Rayleigh and Raman scattering peaks were removed computationally.[73] Absorption of PM extracts in the range λ_{ex} = 200-600 nm was recorded to correct the EEM measurements for inner filter effect.[74] The processed EEMs were then passed through a median filter and a Gaussian filter in MATLAB (MathWorks Inc.) to smooth the data.

174 4.5. Principal Component Regression (PCR)

175 PCR was performed as a two-step process: (1) transforming the EEM data onto its principal
176 components (PCs) and (2) fitting regression models on the transformed EEM data and PAH
177 concentrations obtained from GCMS analysis. EEM is recorded as a 2D matrix with a fluorescence
178 intensity value for each pixel which corresponds to one of 1000 row positions (one for each
179 emission wavelength) and 201 column positions (one for each excitation wavelength).

180 In the first step of PCR, each EEM 2D matrix (1000 x 201) was unfolded into a 1D row vector (1
181 x 20100). The EEM row vectors of all samples were stacked to create a data matrix C (n x 201000),
182 where n is the total number of samples. The data matrix C was reduced with principal component
183 analysis (PCA) using the scikit-learn library in Python 3.6.0.[75] The number of PCs (d), required to
184 represent the data in the data matrix C was varied from 1 to 10. The data matrix C can be
185 represented as the matrix product of s and v and a residual matrix E, shown in (1)

$$C = sv + E \quad (1)$$

186 where s (n x d) is the scores matrix and v (d x 201000) is the loadings matrix having d PC vectors.
187 The scores matrix s is the reduced form of data matrix C; the operation reduces the number of data
188 points required to represent each EEM from 20100 to d. The value of d is chosen to minimize the
189 number of PCs that account for the maximum variance in the EEM dataset. The variance in the
190 EEM data accounted by the PCs for d=1 to 10, see Figure S16.

191 For the second step of PCR, the scores matrix s (n x d) is used to fit linear models for estimating
192 concentrations of PAH fractions. We used the ordinary least squares method in the scikit-learn

library in Python 3.6.0 to perform multiple linear regression (MLR) to fit two linear models between: (i) EEM scores matrix and the LMW PAH concentrations from GCMS analysis and (ii) EEM scores matrix and HMW PAH concentrations from GCMS analysis. The mean squared error (MSE) representing the error in correlation for each model was calculated using "leave one out cross-validation" method (LOOCV).[75] The MSEs for range d=1-10 are shown in Figure S17. Based on the variance in the EEM data for d=1- 10 PCs and the MSE, $d = 5$ was chosen for fitting the linear models as it accounted for 99.99% variance. The MSE did not change significantly for $d > 5$, indicating that all relevant spectral features were captured by the first 5 PCs.

Finally, PCA and MLR, referred together as principal component regression (PCR), was performed using all samples (n=20) and $d = 5$. The coefficient of determination (R^2) was determined using LOOCV.

5. Results and Discussion

5.1. Effect of Fuel Dilution on the Soot Yields and TOC

Effect of fuel dilution by Ar on the maximum flame temperatures, soot yields, and TOC is studied. Figure 1A shows that T_{max} decreases with fuel dilution due to heat transfer from the combustion reaction to Ar. The flame brightness and color are shown in Figure S6 and Figure S7. Figure 1B shows that the emission factor increases with T_{max}. The amount of soot produced for the flame condition with the highest T_{max} is two orders of magnitude greater than that of the lowest temperature. Although the emission factor is measured ex-situ gravimetrically, visual observation confirms that flames with greater T_{max} have significantly higher soot radiation. At the higher Ar dilutions, the flame is mostly blue (Figure S6 and Figure S7) with a visible orange region at the tip of the flame. This agrees with the previous reports of soot formation suppression due to inert

additives.[76] The contributing factors include (i) dilution (lower concentrations) of species participating in the reaction, (ii) thermal effects – lower collision energies, and (iii) chemical effects caused by the free radicals scavenging by the diluent. Dilution by inert additives has been shown to have a greater impact on the sooting tendency than thermal effects alone.[76–78]

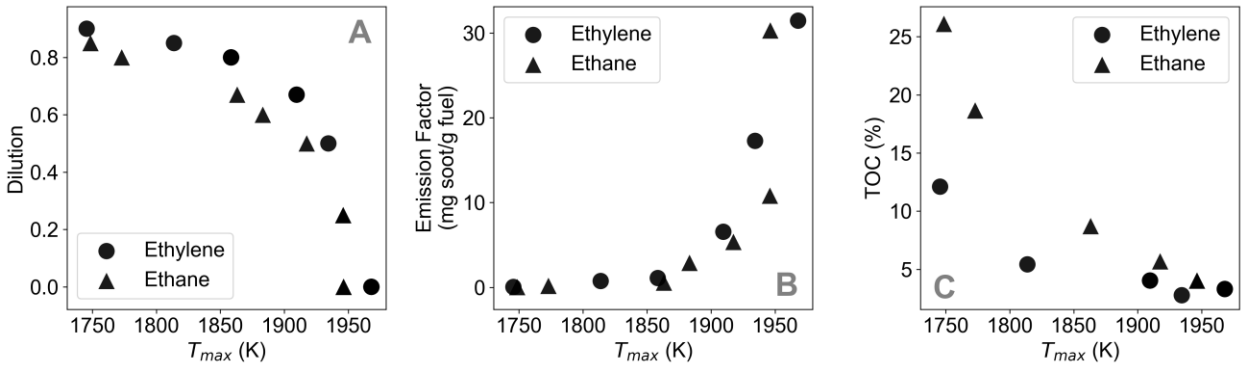

Figure 1: Maximum flame temperature (T_{max}) varies with argon dilution of fuel affecting the soot emission factor and TOC from ethylene and ethane flames. (A): The maximum flame temperature decreases with increasing Ar dilution for both fuels. (B): The emission factor (soot yields) increases with flame temperature. (C): TOC fraction decreases with increasing flame temperature. Figure S8 shows variation of soot emission factor and TOC with Ar dilution for both fuels.

Figure 1C shows that TOC decreases with the increase in flame temperature. The higher TOC in the soot from lower temperature flames is likely due to reduction in hydrogen abstraction, hindrance of carbonization of young soot particles and reduction in PAH oxidation rates.[20] Detailed analysis of the soot formation mechanisms and the effects of the flame conditions on the PM composition[79,80] are beyond the scope of this work.

5.2. PAH Composition from GCMS Analysis

Figure 2 shows the PAH content in PM generated from ethylene and ethane flames as a function of flame temperatures. A total of 24 PAHs were analysed, but only 16 groups are shown, as the PAHs detected at low concentrations were excluded, and structural isomers were grouped together. For both fuels, HMW PAHs are observed at lower T_{max}. The LMW PAHs are mostly found at intermediate and high T_{max}. Curiously, in ethylene's case, lowest T_{max} conditions yield both LMW and some HMW PAHs associated with PM. We do not have an explanation for this observation though this data point was repeated several times. Figure S9 and Figure S10 show the complete GCMS dataset including each PAH compound.

For both fuels, we observe two temperature ranges that correspond to the presence of HMW and LMW PAHs in the PM sample. The transition is associated with soot maturation, i.e., a transition of nascent soot with liquid-like properties, high organic fraction and unstructured morphology to particles with graphitic core-shell carbon structures. This transition is typically defined by carbonization temperature (T_{carb})[81,82]. From a phenomenological perspective, the temperature in the highest soot concentration region is a more relevant metric to evaluate this transition than the maximum flame temperature. In our experiments, T_{max} is always higher than the temperature experienced by the soot during maturation T^*. The values of T^* were determined based on the temperature range in the highest luminosity region in flame images, estimated using thermocouple temperature measurements along the flame front; the details are described in SI Section 4. For flames with $T^* > T_{carb}$, the liquid-like HMW PAHs that form the nascent soot particle, transition to graphitic structures forming black carbon (BC), which is typically associated with high-temperature combustion sources. Brown carbon, characterized by high TOC fraction, is often found in low-temperature combustion. These conditions are typically present in biomass

combustion due to lower heating value of the fuel (high moisture content) and complex (endothermic) surface chemistry reaction. In our experiments, lower temperature samples exhibit a brown color. In terms of maximum flame temperature, the threshold for transition from high PAH PM to highly graphitic PM is in the range 1814K-1864K, denoted by $T_{max,c}$, the subscript 'c' stands for critical. The transition is shown as a dotted grey line in Figure 2. These flame temperatures correspond to the estimated local temperature condition for soot exposure of T^*_c ~ 1600K-1650K.

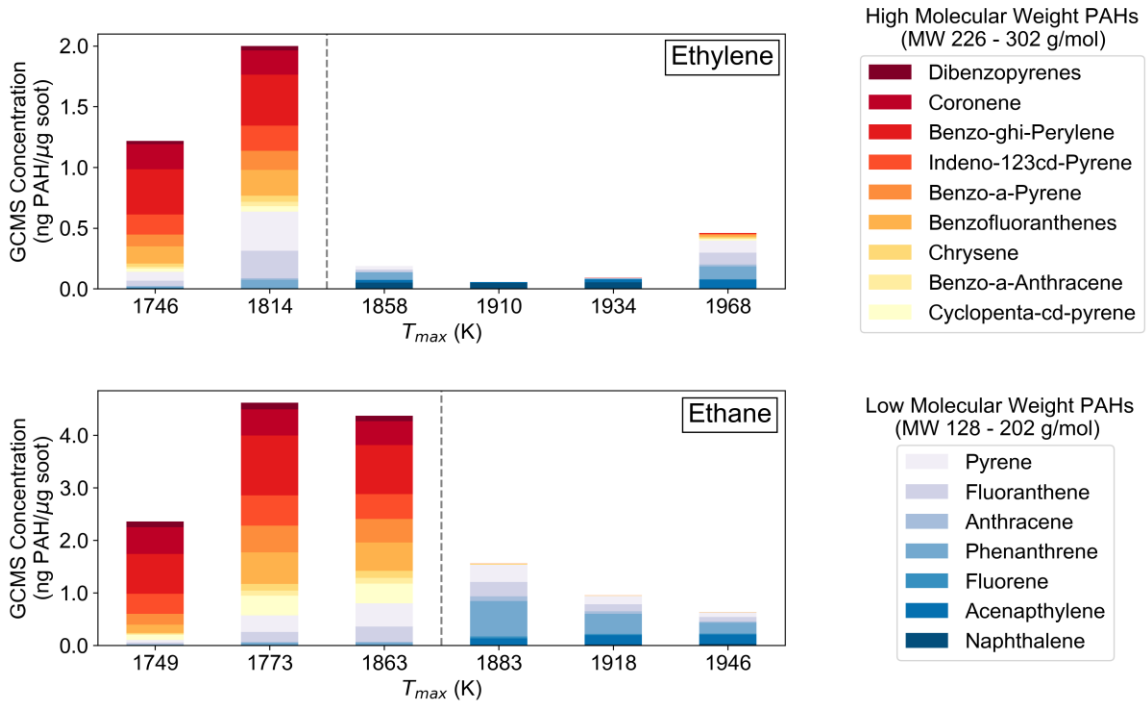

Figure 2: PM PAH fraction as a function of T_{max} for ethylene and ethane flames. GCMS concentration of 16 PAHs is divided into LMW and HMW PAH. For higher $T_{max,}$ LMW PAHs are prevalent; for lower T_{max}, HMW PAHs are the dominant group. The vertical dashed gray line indicates the carbonization threshold in terms of maximum flame temperature.

5.3. Spectral Information from EEM Analysis

Figure 3 shows the EEM spectra of PM generated from ethylene flames at T_{max}=1746K, 1858K and 1968K and ethane flames at T_{max}=1749K, 1863K and 1946K. For both fuels, the location and intensity of fluorescence emission peaks varies with T_{max}. At T_{max}=1968K for ethylene and T_{max}=1946K for ethane, the emission peaks are present at shorter excitation wavelengths and have lower intensities. At T_{max}=1746K for ethylene and T_{max}=1749K for ethane, the range of excitation wavelengths where fluorescence peaks are observed increases, indicating a broadening of PAH absorption bands, and the emission peaks shift towards longer wavelengths. This suggests that colder flames produce PM with higher MW PAHs than hotter (less diluted) flames, which agrees with the GCMS analysis, as shown in Figure 2. The EEM spectra for the entire range of flame conditions are shown in Figure S12. Figure S14 shows the emission spectra for pure PAHs in the target molecular weight range. By comparison, the emission peaks in the EEMs from higher T_{max} samples are associated with the LMW PAHs and emission peaks in the EEMs for PM samples at lower T_{max} are associated with the HMW PAHs. Similar to the GCMS data, the temperature threshold can be determined by change in the EEM spectra. Note that the EEM signal intensities are significantly greater for lower temperature samples due to the high fluorescence quantum yield of HMW PAHs (sample mass normalized).[83] The odd result of having HMW PAHs for the hottest ethylene condition, T_{max}=1968K, as pointed out in the GCMS analysis, is also observed in EEM analysis via the fluorescence peaks associated with HMW PAHs at λ_{ex} = 300 – 400 nm and λ_{em} = 400 – 500 nm.

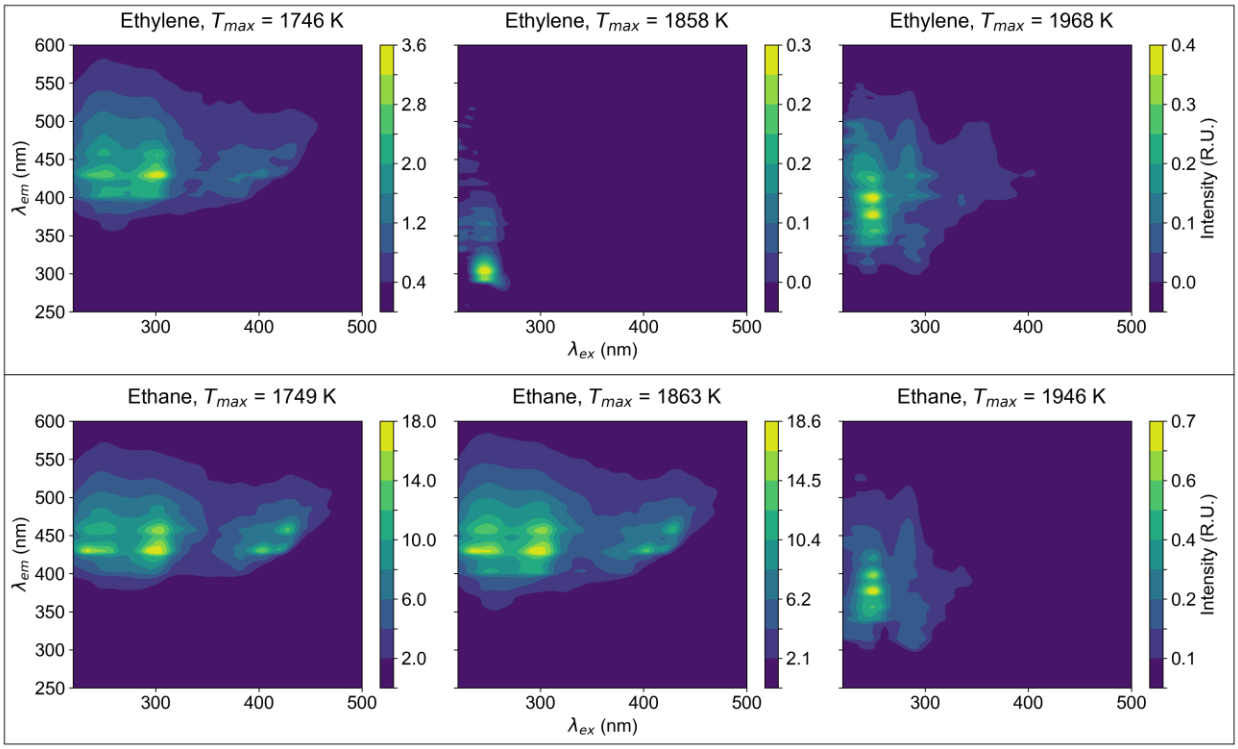

Figure 3: The location and intensity of fluorescence peaks in the EEM spectra vary with T_{max}. PM samples for hotter flames have emission peaks at shorter emission wavelengths and in narrow excitation bands. PM samples at lower T_{max} have emission peaks at longer emission wavelengths and broader excitation bands.

5.4. Total Fluorescence Intensity

Figure 4 compares the total PAH concentrations in PM samples from GCMS analysis against the total fluorescence intensity, defined as the sum of intensities at each excitation-emission pair in the EEM. Since PM samples from $T_{max} > T_{max,c}$ have predominantly LMW PAHs (see Figure 2), variation in the total fluorescence intensity can be attributed to the variation in predominantly LMW PAH concentrations. LMW PAH fluorescence peaks are located in the lower-left quadrant

of the EEM spectra at shorter excitation and emission wavelengths ($\lambda_{ex} < 300nm; \lambda_{em} < 450nm$), as shown in Figure 3. Similarly, variation in the total fluorescence intensity in PM samples for $T_{max} < T_{max,c}$ can be attributed to the variation in concentrations of HMW PAHs; their fluorescence peaks located at higher wavelengths ($\lambda_{ex} > 300nm;\ \lambda_{em} > 400nm$). There is a clear distinction between emission wavelength and width of excitation bands in the EEMs of PM samples with dominant LMW PAHs vs. HMW PAHs. The integrated fluorescence intensity follows the total PAH concentration levels for both fuels over a wide range of flame temperatures. Compounds other than the 24 PAHs from GCMS panel contribute to the fluorescence, their peak location in the EEM spectra and relative intensity are not known.

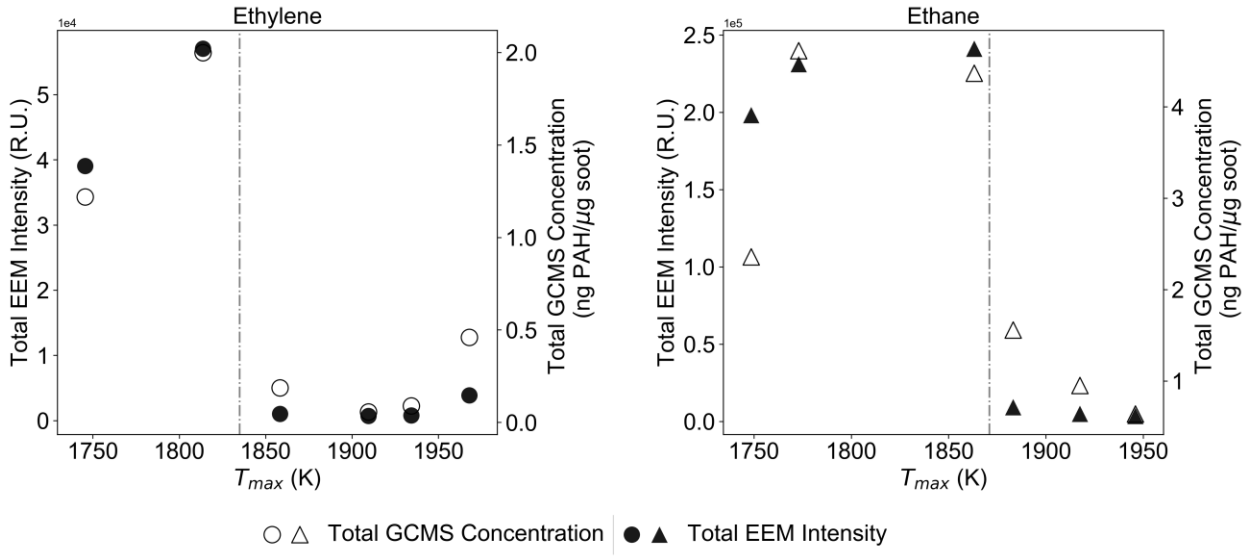

Figure 4: Comparison of integrated EEM fluorescence signal to PAH concentration from GCMS analysis of 24 PAHs panel for diluted ethylene and ethane flames. The dotted line represents transition threshold from black carbon (low TOC, low HMW PAHs) to brown carbon (high TOC, high HMW PAHs).

5.5. Correlating EEM and GCMS Results

Figure 5 shows the estimated LMW and HMW PAH concentrations based on the EEM-PCR analysis with five principal components. Based on the LOOCV method, the correlations with GCMS data have R^2 values of 0.98 and 0.99 for the LMW and HMW PAH, respectively. Although the intensity of the EEM fluorescence peaks for high-temperature PM samples is lower than that for colder flames (see Figure 4), the unique attributes of the spectra, i.e., peak locations, widths, and other overall shape parameters, allow for accurate estimation of LMW PAH concentrations.

Here we propose that fluorescence intensity in the specific EEM region, indicative of the concentration of LMW and HMW PAHs, can be used as a fluorescent fingerprint for the organic compounds in combustion PM. For samples where both LMW and HMW PAH groups are present, their emission wavelengths and excitation bands overlap, and it is necessary to determine the fraction of each group. In the current work, the PCR technique is used to extract features associated with LMW and HMW PAHs and to determine the concentration of each PAH group. While this method can estimate LMW and HMW PAH concentrations as low as 0.1 ng PAH/μg soot, it is not specific in terms of determining the concentrations of individual PAHs due to the overlap in fluorescence peaks and presence of other fluorescent species which were not analyzed in the present study. Multivariate analysis techniques can improve the accuracy and specificity of this method if the data includes a greater variation in concentration of the specific PAH target.

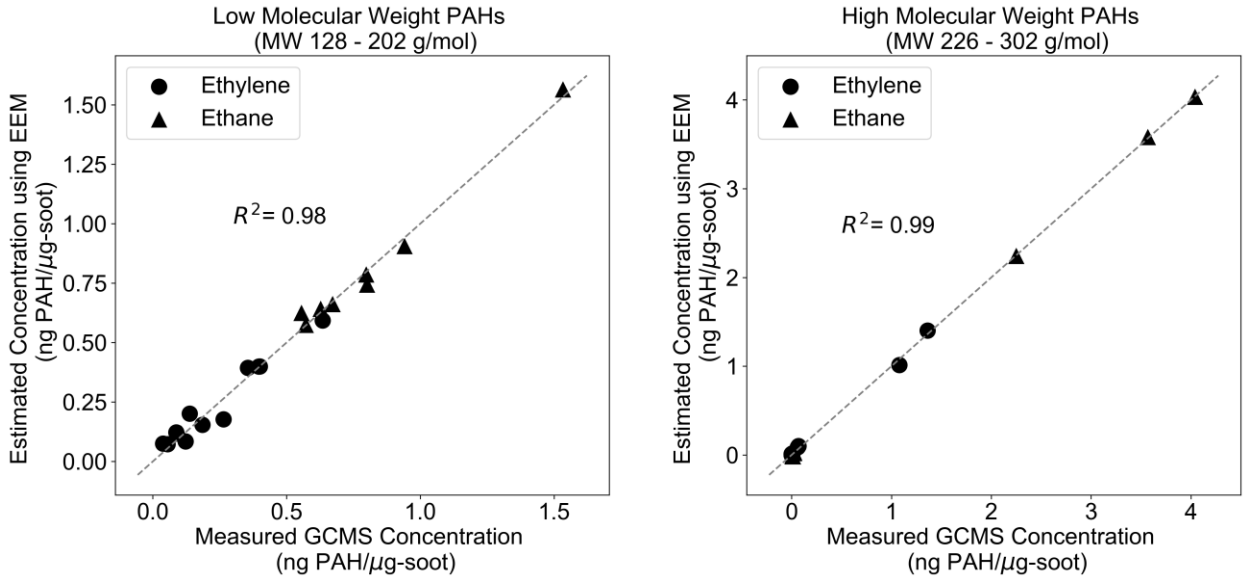

Figure 5: Parity plots of PAH concentrations estimated by EEM-PCR vs. concentration measured by GCMS for LMW (left) and HMW (right) PAHs in PM samples generated from ethylene and ethane flames.

In this study, we have demonstrated that the PCR-EEM technique can be used to estimate combustion PM organic fraction, in particular, the concentrations of LMW and HMW PAH groups. Composition of combustion PM in terms of TOC and PAH concentrations was controlled by Ar dilution of ethylene and ethane in the inverted gravity diffusion flame. The maximum flame temperature decreases with increase in fuel dilution. The colder flames produce lower PM yield; however, the PM TOC content increased significantly, from 3-5% up to 13-27% for ethylene and ethane respectively. The increase in organic carbon is associated with the presence of HMW PAHs. Temperature thresholds for PM transition from low to high TOC PM were determined based on the maximum flame temperature $T_{max,c}$ ~1814-1864K, which corresponds to temperature of the highest soot luminosity (concentration) region of T^*_c~1600-1650K. The PCR-EEM method based

on fluorescent fingerprint attributes, such as location, width, overall shape and intensity can be used to quantify the levels of LMW and HMW PAH groups in ultrafine PM produced by combustion.

6. Acknowledgements

This work was supported by the National Institute of Health grants U01 EB021923 and NIEHS R42ES026532 subcontract to the University of Washington.

7. References

(1) Popovicheva, O.; Kistler, M.; Kireeva, E.; Persiantseva, N.; Timofeev, M.; Kopeikin, V.; Kasper-Giebl, A. Physicochemical Characterization of Smoke Aerosol during Large-Scale Wildfires: Extreme Event of August 2010 in Moscow. *Atmos. Environ.* **2014**, *96*, 405–414. https://doi.org/10.1016/j.atmosenv.2014.03.026.

(2) Chakrabarty, R. K.; Beres, N. D.; Moosmüller, H.; China, S.; Mazzoleni, C.; Dubey, M. K.; Liu, L.; Mishchenko, M. I. Soot Superaggregates from Flaming Wildfires and Their Direct Radiative Forcing. *Sci. Rep.* **2014**, *4*, 5508. https://doi.org/10.1038/srep05508.

(3) Goodarzi, F. Morphology and Chemistry of Fine Particles Emitted from a Canadian Coal-Fired Power Plant. *Fuel* **2006**, *85* (3), 273–280. https://doi.org/10.1016/j.fuel.2005.07.004.

(4) Köylü, Ü. Ö.; Faeth, G. M. Structure of Overfire Soot in Buoyant Turbulent Diffusion Flames at Long Residence Times. *Combust. Flame* **1992**, *89* (2), 140–156. https://doi.org/10.1016/0010-2180(92)90024-J.

(5) Lin, P.; Fleming, L. T.; Nizkorodov, S. A.; Laskin, J.; Laskin, A. Comprehensive Molecular Characterization of Atmospheric Brown Carbon by High Resolution Mass

Spectrometry with Electrospray and Atmospheric Pressure Photoionization. *Anal. Chem.* **2018**, *90* (21), 12493–12502. https://doi.org/10.1021/acs.analchem.8b02177.

(6) WHO | Mortality and burden of disease from ambient air pollution https://www.who.int/gho/phe/outdoor_air_pollution/burden_text/en/ (accessed Mar 10, 2019).

(7) Steenhof, M.; Gosens, I.; Strak, M.; Godri, K. J.; Hoek, G.; Cassee, F. R.; Mudway, I. S.; Kelly, F. J.; Harrison, R. M.; Lebret, E.; et al. In Vitro Toxicity of Particulate Matter (PM) Collected at Different Sites in the Netherlands Is Associated with PM Composition, Size Fraction and Oxidative Potential - the RAPTES Project. *Part. Fibre Toxicol.* **2011**, *8* (1), 26. https://doi.org/10.1186/1743-8977-8-26.

(8) VALAVANIDIS, A.; FIOTAKIS, K.; VLACHOGIANNI, T. Airborne Particulate Matter and Human Health: Toxicological Assessment and Importance of Size and Composition of Particles for Oxidative Damage and Carcinogenic Mechanisms. *J. Environ. Sci. Health Part C* **2008**, *26* (4), 339–362. https://doi.org/10.1080/10590500802494538.

(9) Kim Yong Ho; Warren Sarah H.; Krantz Q. Todd; King Charly; Jaskot Richard; Preston William T.; George Barbara J.; Hays Michael D.; Landis Matthew S.; Higuchi Mark; et al. Mutagenicity and Lung Toxicity of Smoldering vs. Flaming Emissions from Various Biomass Fuels: Implications for Health Effects from Wildland Fires. *Environ. Health Perspect. 126* (1), 017011. https://doi.org/10.1289/EHP2200.

(10) Bell Michelle L.; Dominici Francesca; Ebisu Keita; Zeger Scott L.; Samet Jonathan M. Spatial and Temporal Variation in PM2.5 Chemical Composition in the United States for Health Effects Studies. *Environ. Health Perspect.* **2007**, *115* (7), 989–995. https://doi.org/10.1289/ehp.9621.

(11) Atkinson, R. W.; Mills, I. C.; Walton, H. A.; Anderson, H. R. Fine Particle Components and Health—a Systematic Review and Meta-Analysis of Epidemiological Time Series Studies of Daily Mortality and Hospital Admissions. *J. Expo. Sci. Environ. Epidemiol.* **2015**, *25* (2), 208–214. https://doi.org/10.1038/jes.2014.63.

(12) Baird, W. M.; Hooven, L. A.; Mahadevan, B. Carcinogenic Polycyclic Aromatic Hydrocarbon-DNA Adducts and Mechanism of Action. *Environ. Mol. Mutagen.* **2005**, *45* (2–3), 106–114. https://doi.org/10.1002/em.20095.

(13) Kim Oanh, N. T.; Nghiem, L. H.; Phyu, Y. L. Emission of Polycyclic Aromatic Hydrocarbons, Toxicity, and Mutagenicity from Domestic Cooking Using Sawdust Briquettes, Wood, and Kerosene. *Environ. Sci. Technol.* **2002**, *36* (5), 833–839. https://doi.org/10.1021/es011060n.

(14) de Kok, T. M. C. M.; Driece, H. A. L.; Hogervorst, J. G. F.; Briedé, J. J. Toxicological Assessment of Ambient and Traffic-Related Particulate Matter: A Review of Recent Studies. *Mutat. Res. Mutat. Res.* **2006**, *613* (2), 103–122. https://doi.org/10.1016/j.mrrev.2006.07.001.

(15) Becker, S.; Dailey, L. A.; Soukup, J. M.; Grambow, S. C.; Devlin, R. B.; Huang, Y.-C. T. Seasonal Variations in Air Pollution Particle-Induced Inflammatory Mediator Release and Oxidative Stress. *Environ. Health Perspect.* **2005**, *113* (8), 1032–1038. https://doi.org/10.1289/ehp.7996.

(16) Kim, K.-H.; Jahan, S. A.; Kabir, E.; Brown, R. J. C. A Review of Airborne Polycyclic Aromatic Hydrocarbons (PAHs) and Their Human Health Effects. *Environ. Int.* **2013**, *60*, 71–80. https://doi.org/10.1016/j.envint.2013.07.019.

(17) Richter, H.; Howard, J. B. Formation of Polycyclic Aromatic Hydrocarbons and Their Growth to Soot—a Review of Chemical Reaction Pathways. *Prog. Energy Combust. Sci.* **2000**, *26* (4), 565–608. https://doi.org/10.1016/S0360-1285(00)00009-5.

(18) McEnally, C. S.; Pfefferle, L. D.; Atakan, B.; Kohse-Höinghaus, K. Studies of Aromatic Hydrocarbon Formation Mechanisms in Flames: Progress towards Closing the Fuel Gap. *Prog. Energy Combust. Sci.* **2006**, *32* (3), 247–294. https://doi.org/10.1016/j.pecs.2005.11.003.

(19) Frenklach, M. Reaction Mechanism of Soot Formation in Flames. *Phys. Chem. Chem. Phys.* **2002**, *4* (11), 2028–2037. https://doi.org/10.1039/B110045A.

(20) Wang, H. Formation of Nascent Soot and Other Condensed-Phase Materials in Flames. *Proc. Combust. Inst.* **2011**, *33* (1), 41–67. https://doi.org/10.1016/j.proci.2010.09.009.

(21) Happold, J.; Grotheer, H.-H.; Aigner, M. Distinction of Gaseous Soot Precursor Molecules and Soot Precursor Particles through Photoionization Mass Spectrometry. *Rapid Commun. Mass Spectrom.* **2007**, *21* (7), 1247–1254. https://doi.org/10.1002/rcm.2955.

(22) Davis, J.; Tiwari, K.; Novosselov, I. Soot Morphology and Nanostructure in Complex Flame Flow Patterns via Secondary Particle Surface Growth. *Fuel* **2019**, *245*, 447–457. https://doi.org/10.1016/j.fuel.2019.02.058.

(23) Cao, J. J.; Lee, S. C.; Ho, K. F.; Zou, S. C.; Fung, K.; Li, Y.; Watson, J. G.; Chow, J. C. Spatial and Seasonal Variations of Atmospheric Organic Carbon and Elemental Carbon in Pearl River Delta Region, China. *Atmos. Environ.* **2004**, *38* (27), 4447–4456. https://doi.org/10.1016/j.atmosenv.2004.05.016.

(24) Chow, J. C.; Watson, J. G.; Chen, L.-W. A.; Rice, J.; Frank, N. H. Quantification of PM2.5 Organic Carbon Sampling Artifacts in US Networks. *Atmospheric Chem. Phys.* **2010**, *10* (12), 5223–5239. https://doi.org/10.5194/acp-10-5223-2010.

(25) Baldauf, R. W.; Devlin, R. B.; Gehr, P.; Giannelli, R.; Hassett-Sipple, B.; Jung, H.; Martini, G.; McDonald, J.; Sacks, J. D.; Walker, K. Ultrafine Particle Metrics and Research Considerations: Review of the 2015 UFP Workshop. *Int. J. Environ. Res. Public. Health* **2016**, *13* (11), 1054. https://doi.org/10.3390/ijerph13111054.

(26) Wei, Y.; Han, I.-K.; Hu, M.; Shao, M.; Zhang, J.; Tang, X. Personal Exposure to Particulate PAHs and Anthraquinone and Oxidative DNA Damages in Humans. *Chemosphere* **2010**, *81* (10), 1280–1285. https://doi.org/10.1016/j.chemosphere.2010.08.055.

(27) Bonetta, Sa.; Gianotti, V.; Bonetta, Si.; Gosetti, F.; Oddone, M.; Gennaro, M. C.; Carraro, E. DNA Damage in A549 Cells Exposed to Different Extracts of PM2.5 from Industrial, Urban and Highway Sites. *Chemosphere* **2009**, *77* (7), 1030–1034. https://doi.org/10.1016/j.chemosphere.2009.07.076.

(28) Wei, Y.; Han, I.-K.; Shao, M.; Hu, M.; Zhang, J. (Jim); Tang, X. PM2.5 Constituents and Oxidative DNA Damage in Humans. *Environ. Sci. Technol.* **2009**, *43* (13), 4757–4762. https://doi.org/10.1021/es803337c.

(29) *Office of the Federal Registration (OFR) Appendix A: Priority Pollutants. Fed Reg. 1982;47:52309.*

(30) Samburova, V.; Zielinska, B.; Khlystov, A. Do 16 Polycyclic Aromatic Hydrocarbons Represent PAH Air Toxicity? *Toxics* **2017**, *5* (3). https://doi.org/10.3390/toxics5030017.

(31) *Some Non-Heterocyclic Polycyclic Aromatic Hydrocarbons and Some Related Occupational Exposures*; IARC Working Group on the Evaluation of Carcinogenic Risks to Humans, International Agency for Research on Cancer, Eds.; IARC monographs on the evaluation of carcinogenic risks to humans; IARC Press ; Distributed by World Health Organization: Lyon, France : Geneva, 2010.

(32) National Toxicology Program: 14th Report on Carcinogens https://ntp.niehs.nih.gov/go/roc14 (accessed Mar 12, 2019).

(33) *Canadian Sediment Quality Guidelines for the Protection of Aquatic Life - Polycyclic Aromatic Hydrocarbons*; Canadian Council of Ministers of the Environment, 1999; p 16.

(34) Wornat, M. J.; Ledesma, E. B.; Sandrowitz, A. K.; Roth, M. J.; Dawsey, S. M.; Qiao, Y.-L.; Chen, W. Polycyclic Aromatic Hydrocarbons Identified in Soot Extracts from Domestic Coal-Burning Stoves of Henan Province, China. *Environ. Sci. Technol.* **2001**, *35* (10), 1943–1952. https://doi.org/10.1021/es001664b.

(35) An, Y.; Teng, S.; Pei, Y.; Qin, J.; Li, X.; Zhao, H. An Experimental Study of Polycyclic Aromatic Hydrocarbons and Soot Emissions from a GDI Engine Fueled with Commercial Gasoline. *Fuel* **2016**, *164*, 160–171. https://doi.org/10.1016/j.fuel.2015.10.007.

(36) Hutzler, C.; Luch, A.; Filser, J. G. Analysis of Carcinogenic Polycyclic Aromatic Hydrocarbons in Complex Environmental Mixtures by LC-APPI-MS/MS. *Anal. Chim. Acta* **2011**, *702* (2), 218–224. https://doi.org/10.1016/j.aca.2011.07.003.

(37) Bergauff, M.; Ward, T.; Noonan, C.; Palmer, C. P. Determination and Evaluation of Selected Organic Chemical Tracers for Wood Smoke in Airborne Particulate Matter. *Int. J. Environ. Anal. Chem.* **2008**, *88* (7), 473–486. https://doi.org/10.1080/03067310701809110.

(38) Lin, P.; Fleming, L. T.; Nizkorodov, S. A.; Laskin, J.; Laskin, A. Comprehensive Molecular Characterization of Atmospheric Brown Carbon by High Resolution Mass Spectrometry with Electrospray and Atmospheric Pressure Photoionization. *Anal. Chem.* **2018**, *90* (21), 12493–12502. https://doi.org/10.1021/acs.analchem.8b02177.

(39) Faccinetto, A.; Focsa, C.; Desgroux, P.; Ziskind, M. Progress toward the Quantitative Analysis of PAHs Adsorbed on Soot by Laser Desorption/Laser Ionization/Time-of-Flight Mass Spectrometry. *Environ. Sci. Technol.* **2015**, *49* (17), 10510–10520. https://doi.org/10.1021/acs.est.5b02703.

(40) Skeen, S. A.; Michelsen, H. A.; Wilson, K. R.; Popolan, D. M.; Violi, A.; Hansen, N. Near-Threshold Photoionization Mass Spectra of Combustion-Generated High-Molecular-Weight Soot Precursors. *J. Aerosol Sci.* **2013**, *58*, 86–102. https://doi.org/10.1016/j.jaerosci.2012.12.008.

(41) Andrade-Eiroa, A.; Shahla, R.; Romanías, M. N.; Dagaut, P. An Alternative to Trial and Error Methodology in Solid Phase Extraction: An Original Automated Solid Phase Extraction Procedure for Analysing PAHs and PAH-Derivatives in Soot. *RSC Adv.* **2014**, *4* (63), 33636–33644. https://doi.org/10.1039/C4RA03214D.

(42) Wartel, M.; Pauwels, J.-F.; Desgroux, P.; Mercier, X. Quantitative Measurement of Naphthalene in Low-Pressure Flames by Jet-Cooled Laser-Induced Fluorescence. *Appl. Phys. B* **2010**, *100* (4), 933–943. https://doi.org/10.1007/s00340-010-4135-2.

(43) Garra, P.; Maschowski, C.; Liaud, C.; Dieterlen, A.; Trouvé, G.; Calvé, S. L.; Jaffrezo, J.-L.; Leyssens, G.; Schönnenbeck, C.; Kohler, S.; et al. Fluorescence Microscopy Analysis of Particulate Matter from Biomass Burning: Polyaromatic Hydrocarbons as Main

Contributors. *Aerosol Sci. Technol.* **2015**, *49* (11), 1160–1169. https://doi.org/10.1080/02786826.2015.1107181.

(44) Sousa, G.; Kiselev, D.; Kasparian, J.; George, C.; Ferreira, J.; Favreau, P.; Lazzarotto, B.; Wolf, J.-P. Time-Resolved Monitoring of Polycyclic Aromatic Hydrocarbons Adsorbed on Atmospheric Particles. *Environ. Sci. Pollut. Res.* **2017**, *24* (24), 19517–19523. https://doi.org/10.1007/s11356-017-9612-2.

(45) Aizawa, T.; Kosaka, H. Effects of Fischer—Tropsch Diesel Fuel on Soot Formation Processes in a Diesel Spray Flame. *Int. J. Engine Res.* **2010**, *11* (1), 79–87. https://doi.org/10.1243/14680874JER04709.

(46) Reilly, P. T. A.; Gieray, R. A.; Whitten, W. B.; Ramsey, J. M. Direct Observation of the Evolution of the Soot Carbonization Process in an Acetylene Diffusion Flame via Real-Time Aerosol Mass Spectrometry. *Combust. Flame* **2000**, *122* (1), 90–104. https://doi.org/10.1016/S0010-2180(00)00105-X.

(47) Berlman, I. *Handbook of Florescence Spectra of Aromatic Molecules*; Elsevier, 2012.

(48) Robertson, J.; O'Reilly, E. P. Electronic and Atomic Structure of Amorphous Carbon. *Phys. Rev. B* **1987**, *35* (6), 2946–2957. https://doi.org/10.1103/PhysRevB.35.2946.

(49) Menon, A.; Dreyer, J. A. H.; Martin, J. W.; Akroyd, J.; Robertson, J.; Kraft, M. Optical Band Gap of Cross-Linked, Curved, and Radical Polyaromatic Hydrocarbons. *Phys. Chem. Chem. Phys.* **2019**, *21* (29), 16240–16251. https://doi.org/10.1039/C9CP02363A.

(50) Martin, J. W.; Bowal, K.; Menon, A.; Slavchov, R. I.; Akroyd, J.; Mosbach, S.; Kraft, M. Polar Curved Polycyclic Aromatic Hydrocarbons in Soot Formation. *Proc. Combust. Inst.* **2019**, *37* (1), 1117–1123. https://doi.org/10.1016/j.proci.2018.05.046.

(51) Birks, J. B. *Photophysics of Aromatic Molecules*; WILEY - INTERSCIENCE a division of John Wiley & Sons Ltd.

(52) Rieger, R.; Müllen, K. Forever Young: Polycyclic Aromatic Hydrocarbons as Model Cases for Structural and Optical Studies. *J. Phys. Org. Chem.* **2010**, *23* (4), 315–325. https://doi.org/10.1002/poc.1644.

(53) Moerner, W. E.; Fromm, D. P. Methods of Single-Molecule Fluorescence Spectroscopy and Microscopy. *Rev. Sci. Instrum.* **2003**, *74* (8), 3597–3619. https://doi.org/10.1063/1.1589587.

(54) Elcoroaristizabal, S.; de Juan, A.; García, J. A.; Durana, N.; Alonso, L. Comparison of Second-Order Multivariate Methods for Screening and Determination of PAHs by Total Fluorescence Spectroscopy. *Chemom. Intell. Lab. Syst.* **2014**, *132*, 63–74. https://doi.org/10.1016/j.chemolab.2014.01.005.

(55) L. Nahorniak, M.; S. Booksh, K. Excitation-Emission Matrix Fluorescence Spectroscopy in Conjunction with Multiway Analysis for PAH Detection in Complex Matrices. *Analyst* **2006**, *131* (12), 1308–1315. https://doi.org/10.1039/B609875D.

(56) Rutherford, J.; Dawson-Elli, N.; Manicone, A. M.; Korshin, G. V.; Novosselov, I. V.; Seto, E.; Posner, J. D. Excitation Emission Matrix Fluorescence Spectroscopy for Combustion Generated Particulate Matter Source Identification. *ChemRxiv* **2019**. https://doi.org/10.26434/chemrxiv.9177146.

(57) Aizawa, T.; Kosaka, H. Investigation of Early Soot Formation Process in a Diesel Spray Flame via Excitation—Emission Matrix Using a Multi-Wavelength Laser Source. *Int. J. Engine Res.* **2008**, *9* (1), 79–97. https://doi.org/10.1243/14680874JER01407.

(58) JiJi, R. D.; Cooper, G. A.; Booksh, K. S. Excitation-Emission Matrix Fluorescence Based Determination of Carbamate Pesticides and Polycyclic Aromatic Hydrocarbons. *Anal. Chim. Acta* **1999**, *397* (1), 61–72. https://doi.org/10.1016/S0003-2670(99)00392-X.

(59) Muroski, A. R.; Booksh, K. S.; Myrick, M. L. Single-Measurement Excitation/Emission Matrix Spectrofluorometer for Determination of Hydrocarbons in Ocean Water. 1. Instrumentation and Background Correction. *Anal. Chem.* **1996**, *68* (20), 3534–3538. https://doi.org/10.1021/ac960252b.

(60) Booksh, K. S.; Muroski, A. R.; Myrick, M. L. Single-Measurement Excitation/Emission Matrix Spectrofluorometer for Determination of Hydrocarbons in Ocean Water. 2. Calibration and Quantitation of Naphthalene and Styrene. *Anal. Chem.* **1996**, *68* (20), 3539–3544. https://doi.org/10.1021/ac9602534.

(61) Beltrán, J. L.; Ferrer, R.; Guiteras, J. Multivariate Calibration of Polycyclic Aromatic Hydrocarbon Mixtures from Excitation–Emission Fluorescence Spectra. *Anal. Chim. Acta* **1998**, *373* (2), 311–319. https://doi.org/10.1016/S0003-2670(98)00420-6.

(62) Chen, H.; Liao, Z.; Gu, X.; Xie, J.; Li, H.; Zhang, J. Anthropogenic Influences of Paved Runoff and Sanitary Sewage on the Dissolved Organic Matter Quality of Wet Weather Overflows: An Excitation–Emission Matrix Parallel Factor Analysis Assessment. *Environ. Sci. Technol.* **2017**, *51* (3), 1157–1167. https://doi.org/10.1021/acs.est.6b03727.

(63) Osburn, C. L.; Handsel, L. T.; Peierls, B. L.; Paerl, H. W. Predicting Sources of Dissolved Organic Nitrogen to an Estuary from an Agro-Urban Coastal Watershed. *Environ. Sci. Technol.* **2016**, *50* (16), 8473–8484. https://doi.org/10.1021/acs.est.6b00053.

(64) Stipe, C. B.; Higgins, B. S.; Lucas, D.; Koshland, C. P.; Sawyer, R. F. Inverted Co-Flow Diffusion Flame for Producing Soot. *Rev. Sci. Instrum.* **2005**, *76* (2), 023908. https://doi.org/10.1063/1.1851492.

(65) Ghazi, R.; Tjong, H.; Soewono, A.; Rogak, S. N.; Olfert, J. S. Mass, Mobility, Volatility, and Morphology of Soot Particles Generated by a McKenna and Inverted Burner. *Aerosol Sci. Technol.* **2013**, *47* (4), 395–405.

(66) Chakrabarty, R. K.; Novosselov, I. V.; Beres, N. D.; Moosmüller, H.; Sorensen, C. M.; Stipe, C. B. Trapping and Aerogelation of Nanoparticles in Negative Gravity Hydrocarbon Flames. *Appl. Phys. Lett.* **2014**, *104* (24), 243103. https://doi.org/10.1063/1.4884057.

(67) Liu, P.; Arnold, I.; Wang, Y.; Yu, Y.; Fang, J.; Biswas, P.; K. Chakrabarty, R. Synthesis of Titanium Dioxide Aerosol Gels in a Buoyancy-Opposed Flame Reactor. *Aerosol Sci. Technol.* **2015**, *49*, 00–00. https://doi.org/10.1080/02786826.2015.1112356.

(68) Molnar, E. Effects of Temperature and Fuel Dilution on Soot Yields in an Inverted Gravity Flame Reactor. Master of Science in Mechanical Engineering, Univiersity of Washington, Seattle,WA, 2019.

(69) Allen, R.; Box, M.; Liu, L.-J. S.; Larson, T. V. A Cost-Effective Weighing Chamber for Particulate Matter Filters. *J. Air Waste Manag. Assoc.* **2001**, *51* (12), 1650–1653. https://doi.org/10.1080/10473289.2001.10464392.

(70) Birch, M. E. Occupational Monitoring of Particulate Diesel Exhaust by NIOSH Method 5040. *Appl. Occup. Environ. Hyg.* **2002**, *17* (6), 400–405. https://doi.org/10.1080/10473220290035390.

(71) Shang, D.; Kim, M.; Haberl, M. Rapid and Sensitive Method for the Determination of Polycyclic Aromatic Hydrocarbons in Soils Using Pseudo Multiple Reaction Monitoring

Gas Chromatography/Tandem Mass Spectrometry. *J. Chromatogr. A* **2014**, *1334*, 118–125. https://doi.org/10.1016/j.chroma.2014.01.074.

(72) Murphy, K. R.; Butler, K. D.; Spencer, R. G. M.; Stedmon, C. A.; Boehme, J. R.; Aiken, G. R. Measurement of Dissolved Organic Matter Fluorescence in Aquatic Environments: An Interlaboratory Comparison. *Environ. Sci. Technol.* **2010**, *44* (24), 9405–9412. https://doi.org/10.1021/es102362t.

(73) Zepp, R. G.; Sheldon, W. M.; Moran, M. A. Dissolved Organic Fluorophores in Southeastern US Coastal Waters: Correction Method for Eliminating Rayleigh and Raman Scattering Peaks in Excitation–Emission Matrices. *Mar. Chem.* **2004**, *89* (1), 15–36. https://doi.org/10.1016/j.marchem.2004.02.006.

(74) Larsson, T.; Wedborg, M.; Turner, D. Correction of Inner-Filter Effect in Fluorescence Excitation-Emission Matrix Spectrometry Using Raman Scatter. *Anal. Chim. Acta* **2007**, *583* (2), 357–363. https://doi.org/10.1016/j.aca.2006.09.067.

(75) Pedregosa, F.; Varoquaux, G.; Gramfort, A.; Michel, V.; Thirion, B.; Grisel, O.; Blondel, M.; Prettenhofer, P.; Weiss, R.; Dubourg, V.; et al. Scikit-Learn: Machine Learning in Python. *J Mach Learn Res* **2011**, *12*, 2825–2830.

(76) Glassman, I. Sooting Laminar Diffusion Flames: Effect of Dilution, Additives, Pressure, and Microgravity. *Symp. Int. Combust.* **1998**, *27* (1), 1589–1596. https://doi.org/10.1016/S0082-0784(98)80568-7.

(77) Du, D. X.; Axelbaum, R. L.; Law, C. K. The Influence of Carbon Dioxide and Oxygen as Additives on Soot Formation in Diffusion Flames. *Symp. Int. Combust.* **1991**, *23* (1), 1501–1507. https://doi.org/10.1016/S0082-0784(06)80419-4.

(78) Gülder, Ö. L.; Snelling, D. R. Influence of Nitrogen Dilution and Flame Temperature on Soot Formation in Diffusion Flames. *Combust. Flame* **1993**, *92* (1), 115–124. https://doi.org/10.1016/0010-2180(93)90202-E.

(79) Kailasanathan, R. K. A.; Yelverton, T. L. B.; Fang, T.; Roberts, W. L. Effect of Diluents on Soot Precursor Formation and Temperature in Ethylene Laminar Diffusion Flames. *Combust. Flame* **2013**, *160* (3), 656–670. https://doi.org/10.1016/j.combustflame.2012.11.004.

(80) Zhang, Y.; Wang, L.; Liu, P.; Guan, B.; Ni, H.; Huang, Z.; Lin, H. Experimental and Kinetic Study of the Effects of CO2 and H2O Addition on PAH Formation in Laminar Premixed C2H4/O2/Ar Flames. *Combust. Flame* **2018**, *192*, 439–451. https://doi.org/10.1016/j.combustflame.2018.01.050.

(81) Kholghy, M.; Saffaripour, M.; Yip, C.; Thomson, M. J. The Evolution of Soot Morphology in a Laminar Coflow Diffusion Flame of a Surrogate for Jet A-1. *Combust. Flame* **2013**, *160* (10), 2119–2130. https://doi.org/10.1016/j.combustflame.2013.04.008.

(82) Vander Wal, R. L.; Tomasek, A. J. Soot Nanostructure: Dependence upon Synthesis Conditions. *Combust. Flame* **2004**, *136* (1), 129–140. https://doi.org/10.1016/j.combustflame.2003.09.008.

(83) Serio, N.; Prignano, L.; Peters, S.; Levine, M. Detection of Medium-Sized Polycyclic Aromatic Hydrocarbons via Fluorescence Energy Transfer. *Polycycl. Aromat. Compd.* **2014**, *34* (5), 561–572. https://doi.org/10.1080/10406638.2014.918889.